http://dx.doi.org/10.5012/bkcs.2014.35.5.1356

# Conventional and Inverted Photovoltaic Cells Fabricated Using New Conjugated Polymer Comprising Fluorinated Benzotriazole and Benzodithiophene Derivative

**Ji-Hoon Kim, Chang Eun Song,[†] In-Nam Kang,[‡] Won Suk Shin,[§] Zhi-Guo Zhang,[#] Yongfang Li,[#] and Do-Hoon Hwang[*]**

*Department of Chemistry, and Chemistry Institute for Functional Materials, Pusan National University, Busan 609-735, Korea*
*[*]E-mail: dohoonhwang@pusan.ac.kr*
*[†]Department of Materials Science and Engineering KAIST, Daejeon 305-701, Korea*
*[‡]Department of Chemistry, Catholic University of Korea, Bucheon 420-743, Korea*
*[§]Energy Materials Research Center, Korea Research Institute of Chemical Technology, Daejeon 305-343, Korea*
*[#]Beijing National Laboratory for Molecular Sciences and Key Laboratory of Organic Solids, Institute of Chemistry, Chinese Academy of Sciences, Beijing 100190, China*
*Received November 21, 2013, Accepted January 4, 2014*

A new conjugated copolymer, poly{4,8-bis(triisopropylsilylethynyl)benzo[1,2-*b*:4,5-*b*′]dithiophene-alt-4,7-bis(5-thiophen-2-yl)-5,6-difluoro-2-(heptadecan-9-yl)-2*H*-benzo[*d*][1,2,3]triazole} (PTIPSBDT–DFDTBTz), is synthesized by Stille coupling polycondensation. The synthesized polymer has a band gap energy of 1.9 eV, and it absorbs light in the range 300–610 nm. The hole mobility of a solution-processed organic thin-film transistor fabricated using PTIPSBDT–DFDTBTz is $3.8 \times 10^{-3}$ cm$^2$ V$^{-1}$ s$^{-1}$. Bulk heterojunction photovoltaic cells are fabricated, with a conventional device structure of ITO/PEDOT:PSS/polymer:$PC_{71}BM$/Ca/Al ($PC_{71}BM$ = [6,6]-phenyl-$C_{71}$-butyric acid methyl ester); the device shows a power conversion efficiency (PCE) of 2.86% with an open-circuit voltage ($V_{oc}$) of 0.85 V, a short-circuit current density ($J_{sc}$) of 7.60 mA cm$^{-2}$, and a fill factor (*FF*) of 0.44. Inverted photovoltaic cells with the structure ITO/ethoxylated polyethlyenimine/polymer:$PC_{71}BM$/$MoO_3$/Ag are also fabricated; the device exhibits a maximum PCE of 2.92%, with a $V_{oc}$ of 0.89 V, a $J_{sc}$ of 6.81 mA cm$^{-2}$, and an FF of 0.48.

**Key Words :** Fluorine-substituted benzotriazole, Medium band gap semiconducting polymer, Organic photovoltaic cell

## Introduction

Organic photovoltaic (OPV) technology is attracting much attention because it offers the prospect of lightweight, low-cost devices, large-area solution processing, and flexibility.[1] Recently, research efforts in this field have been devoted to improving the power conversion efficiencies (PCEs) of devices through the design of new materials, device engineering, and the use of new processing techniques.[2] Accordingly, OPV devices based on conjugated polymers as electron donor materials, blended with fullerene derivatives as electron acceptor materials, have achieved PCEs of over 8%.[3] Compared with conventional OPVs, inverted OPVs have improved long-term ambient stability and also show higher PCEs in many cases. Clearly, rational design of the molecular structures of photovoltaic materials and optimization of device physics both play a crucial role in the development of highly efficient OPVs.[4-8] Currently, most research is focused on the design and synthesis of conjugated polymers with low band gaps (1.3–1.5 eV), to enable efficient absorption over a broad range of the solar spectrum; other factors to be considered in molecular design include a deeper highest occupied molecular orbital (HOMO) (−5.2 eV or lower) to produce a high open-circuit voltage ($V_{oc}$) and to improve stability against oxidation, and a high hole mobility for efficient charge transportation. Such low band gap polymers typically display strong light absorption spectra up to 600–900 nm, and usually afford an enhanced short-circuit current density ($J_{sc}$). However, medium band gap polymers (with band gaps of 1.7–2.0 eV) can also play an important role in developing efficient OPVs. For example, a medium band gap polymer usually produces a higher Voc than a low band gap polymer does, because of its deeper HOMO energy level.[9,10] Wide band gap polymers also have important applications in tandem OPVs; these involve two (or more) stacked cells with different active layers, each absorbing different parts of the solar spectrum.[11] Poly(3-hexylthiophene) (P3HT) is still the most commonly used medium band gap material for tandem OPVs.[11] However, P3HT has a relatively high-lying HOMO energy level, so the resulting solar cells have low $V_{oc}$ values (≈ 0.6 V) when used with traditional acceptor materials such as [6,6]-phenyl-$C_{61}$–butyric acid methyl ester or [6,6]-phenyl-$C_{71}$-butyric acid methyl ester ($PC_{71}BM$). New medium band gap polymers with respectable photovoltaic performances and relatively simple device fabrication processes are therefore desirable.[12] Recently, we systematically explored a series of new medium band gap conjugated polymers with symmetrical alkyl side chains containing benzotriazole or fluorinated-quinoxaline-containing donor–acceptor (D–A)-type copolymers. We proved that this molecular design is effective for the development of high-performance OPV materials.[11] In particular, PTIPSBDT–DTBTz, composed of

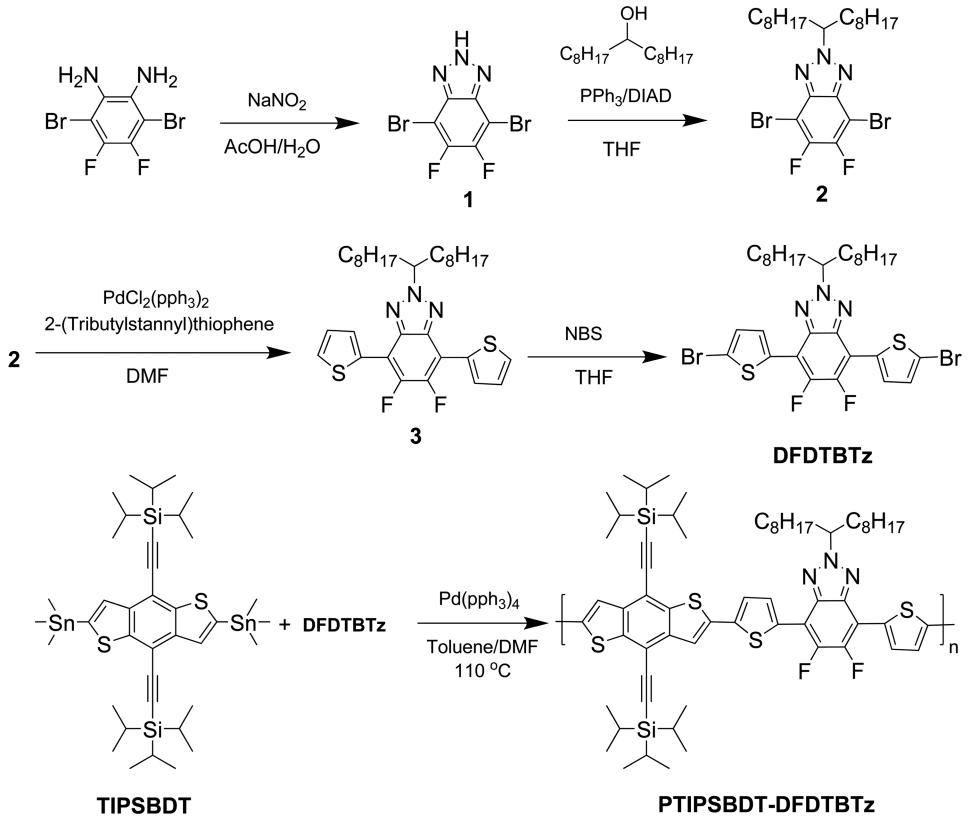


**Scheme 1.** Synthetic routes and chemical structure of PTIPSBDT–DFDTBTz.

4,7-bis(5-bromothiophen-2-yl)-2-(heptadecan-9-yl)-2*H*-benzo[*d*][1,2,3]triazole (DTBTz) and a triisopropylsilylethynyl (TIPS)-substituted benzo[1,2-b:4.5-*b*′]dithiophene (TIPSBDT) unit, with a band gap of 1.95 eV, showed high crystallinity and good photovoltaic performances.[13] In this study, we synthesized a new medium band gap conjugated D–A copolymer, PTIPSBDT–DFDTBTz, consisting of a TIPSBDT donor unit and a fluorinated benzotriazole (DFDTBTz) acceptor unit, for use as donor materials in OPVs. Scheme 1 shows the synthetic routes to the polymers. We expected that the TIPSBDT unit would further lower the HOMO energy level of the resulting polymer by combining with the fluorinated benzotriazole acceptor part. The optical, electrochemical, and photovoltaic properties of PTIPSBDT–DFDTBTz were investigated, in addition to its mobility. Conventional and inverted OPV devices were both fabricated using these conjugated polymers as electron donor materials and $PC_{71}BM$ as the electron acceptor material.

## Experimental

**Materials.** All starting organic compounds were purchased from Aldrich, Alfa Aesar, or TCI Korea, and were used without further purification. TIPSBDT and 3,6-dibromo-4,5-difluorobenzene-1,2-diamine were synthesized according to previously reported methods.[14,15] $PC_{71}BM$ was purchased from EM-index. Solvents were dried and purified by fractional distillation over sodium/benzophenone and handled in a moisture-free atmosphere. Column chromatography was performed using silica gel (Kieselgel 60 63-200 MYM SC, Merck).

**Synthesis of 4,7-Dibromo-5,6-difluoro-2*H*-benzo[*d*][1,2,3]triazole (1).** A solution of sodium nitride (0.27 g, 25.6 mmol) in acetic acid (60 mL) and water (30 mL) was slowly added to a solution of 3,6-dibromo-4,5-difluorobenzene-1,2-diamine (1.00 g, 21.4 mmol). Stirring was continued for 20 min and then the reaction mixture was maintained at room temperature. A pale-pink solid precipitate formed. The mixture was filtered and thoroughly washed with water. The solid was then washed once with cold diethyl ether and purified by flash chromatography to give 1.50 g (80%) of compound **1**. $^1$H NMR (300 MHz, $CDCl_3$) δ 7.50 (s, 2H); $^{13}$C NMR (75 MHz, $CDCl_3$) δ 134.02, 135.13, 115.26. Anal. Calcd for $C_6H_3Br_2N_3$: C, 26.02; H, 1.09; Br, 57.71; N, 15.17; found: C, 25.91; H, 0.99; N, 15.12.

**Synthesis of 4,7-Dibromo-5,6-difluoro-2-(heptadecan-9-yl)-2*H*-benzo[*d*][1,2,3]triazole (2).** Diisopropyl azodicarboxylate (0.77 g, 19.2 mmol) was added to a magnetically stirred solution of **1** (1.00 g, 16.0 mmol), heptadecan-9-ol (1.00 g, 19.2 mmol), and triphenyl phosphine (1.00 g, 19.2 mmol) in tetrahydrofuran (50 mL) at 0 °C under nitrogen. After stirring for 3 h, the reaction mixture was poured into water (200 mL), and the product was extracted with diethyl ether. The organic layer was washed with brine, dried over anhydrous $MgSO_4$, and concentrated under reduced pressure. The crude product was purified by column chromatography and then crystallized from an isopropanol/hexane mixture to give compound **2** as colorless crystals (1.10 g,

50% yield). $^1$H NMR (300 MHz, $CDCl_3$) δ 7.44 (s, 2H), 4.90 (m, 1H), 2.35 (m, 2H), 2.01 (m, 2H), 1.31–1.21 (m, 22H), 1.08–0.96 (m, 2H), 0.86 (t, 6H); $^{13}$C NMR (75 MHz, $CDCl_3$) δ 143.31, 129.22, 110.11, 69.54, 35.59, 31.75, 29.22, 29.14, 29.01, 26.05, 22.62, 14.16. Anal. Calcd. for $C_{23}H_{37}Br_2N_3$: C, 53.60; H, 7.24; Br, 31.01; N, 8.15; found: C, 53.80; H, 7.30; N, 8.10.

**Synthesis of 5,6-Difluoro-2-(heptadecan-9-yl)-4,7-di(thiophen-2-yl)-2*H*-benzo[*d*][1,2,3]triazole (3).** Tripropyl (thiophen-2-yl)stannane (4.50 g, 4.85 mmol) was added to a stirred solution of **2** (3.00 g, 1.90 mmol) and bis(triphenylphosphine)palladium(II)dichloride (0.13 g, 0.06 mmol) in toluene (50 mL). The mixture was refluxed overnight, and then extracted with ethyl acetate. The organic layer was washed with $NaHCO_3$ and brine, and then dried over anhydrous $MgSO_4$. The solvent was removed and the crude product was purified using column chromatography on silica with hexane as the eluent, to yield **3** (3.3 g, 58% yield) as a pale-yellow solid. $^1$H NMR (300 MHz, $CDCl_3$) δ 8.05 (d, 2H), 7.65 (s, 2H), 7.31 (d, 2H), 7.23 (t, 2H), 4.90 (m, 1H), 2.35 (m, 2H), 2.01 (m, 2H), 1.31–1.21 (m, 22H), 1.08–0.96 (m, 2H), 0.86 (t, 6H); $^{13}$C NMR (75 MHz, $CDCl_3$) δ 147.8, 140.2, 132.8, 130.5, 129.2, 125.0, 69.54, 35.59, 31.75, 29.22, 29.14, 29.01, 26.05, 22.62, 14.16. Anal. Calcd. for $C_{31}H_{43}N_3S_2$: C, 71.35; H, 8.31; N, 8.05; S, 12.29; found: C, 70.88; H, 8.25; N, 7.98; S, 12.11.

**Synthesis of 4,7-Bis(5-bromothiophen-2-yl)-5,6-difluoro-2-(heptadecan-9-yl)-2*H*-benzo[*d*][1,2,3]triazole (DFDTBTz).** *N*-Bromosuccinimide (0.7 g, 4.79 mmol) was added to a stirred solution of **3** (1.00 g, 1.92 mmol) in tetrahydrofuran (25 mL) in the absence of light. The mixture was stirred at room temperature for 4 h, and a bright-yellow solid precipitate formed. The mixture was filtered and washed thoroughly with methanol. The solid was then washed once with cold diethyl ether and purified by flash chromatography to give DFDTBTz (1.50 g, 71% yield). $^1$H NMR (300 MHz, $CDCl_3$) δ 7.81 (d, 2H), 7.50 (s, 2H), 7.11 (d, 2H), 4.90 (m, 1H), 2.35 (m, 2H), 2.01 (m, 2H), 1.31–1.21 (m, 22H), 1.08–0.96 (m, 2H), 0.86 (t, 6H); $^{13}$C NMR (75 MHz, $CDCl_3$) δ 147.5, 144.2, 140.5, 135.5, 133.1, 128.0, 115.6, 70.32, 38.61, 35.15, 30.28, 30.10, 29.52, 27.11, 26.32, 12.18. Anal. Calcd. for $C_{31}H_{41}Br_2N_3S_2$: C, 54.79; H, 6.08; N, 6.18; S, 9.44; found: C, 55.01; H, 6.00; N, 5.99; S, 8.74.

**General Polymerization Procedure.** PTIPSBDT–DFDTBTz was synthesized using Stille cross-coupling. A solution of the monomers and tetrakis(triphenylphosphine)palladium in anhydrous toluene (4 mL) and dimethylformamide (DMF; 1 mL) was stirred at 120 °C for 2 d. 2-Bromothiophene and tripropyl(thiophen-2-yl)stannane end-cappers dissolved in anhydrous toluene (1 mL) were added and the mixture was stirred for an additional 12 h. The mixture was then cooled to ~50 °C and poured into methanol (200 mL), with vigorous stirring. The resulting polymer fibers were collected by filtration and further purified by washing with acetone for 2 d in a Soxhlet apparatus to remove any oligomer remnants and catalyst residues, followed by silica gel column chromatography, using chloroform as the eluent. The resulting polymer was soluble in common organic solvents.

**Synthesis of Poly{4,8-Bis(triisopropylsilylethynyl)benzo[1,2-*b*:4,5-*b′*]dithiophene-alt-4,7-bis(5-thiophen-2-yl)-5,6-difluoro-2-(heptadecan-9-yl)-2*H*-benzo[*d*][1,2,3]triazole (PTIPSBDT-DFDTBTz).** The reaction mixture for this polymerization consisted of TIPSBDT (400 mg, 0.27 mmol), DFDTBTz (330 mg, 1.0 equiv), tetrakis(triphenylphosphine)palladium (10 mg, 3.0 μmol), toluene (4 mL), and DMF (1 mL). Anal. Found: C, 71.72; H, 10.17; N, 3.15; S, 6.51.

**Measurements.** $^1$H and $^{13}$C NMR spectra were recorded using a Varian Mercury Plus 300 MHz spectrometer; the chemical shifts were recorded in units of parts per million with CDCl3 as the internal standard. Elemental analysis was performed using a Vario Micro Cube at the Korea Basic Science Institute (Busan, Korea). The absorption spectra were measured using a JASCO JP/V-570 spectrometer. The molecular weights of the polymers were determined via gel permeation chromatography (GPC), relative to a polystyrene standard, using a Waters high-pressure GPC assembly (model M590). Thermogravimetric analyses (TGA) were performed using a Mettler Toledo TGA/SDTA 851e instrument in a nitrogen atmosphere at a heating and cooling rate of 10 °C $min^{-1}$. Cyclic voltammetry (CV) measurements were performed in acetonitrile solution containing 0.1 M tetra-*n*-butylammonium tetrafluoroborate (TBABF4) as the supporting electrolyte, using a CH Instruments electrochemical analyzer with an $Ag/AgNO_3$ reference electrode, platinum wire counter electrode, and platinum working electrode.

**Two-dimensional Grazing-incidence X-ray Scattering (2D-GIXS) Experiments.** 2D-GIXS measurements were performed on 9A beamline of the Pohang Accelerator Laboratory (South Korea). X-rays with wavelengths of 1.1010 Å were used. The chosen incidence angle (~0.15°) allowed complete penetration of the X-rays into the polymer film. A thin layer (40–50 nm) of PEDOT:PSS was spin-coated onto silicon substrates, followed by spin-coating of a layer of the polymer thin films.

**Fabrication of Organic Thin-Film Transistors (OTFTs).** OTFTs were fabricated in a bottom-contact geometry (channel length and width of 12 and 120 μm, respectively). The source and drain contacts were gold (100 nm) and the dielectric was silicon dioxide of thickness 300 nm. The silicon dioxide surface was cleaned, dried, and pretreated with a solution of 10.0 mM octyltrichlorosilane (OTS-8) in toluene at room temperature for 2 h in a nitrogen atmosphere to produce non-polar, smooth surfaces on which to spin-coat the polymers. Chlorobenzene solutions of the polymers (0.5 wt %) were spin-coated at 1000 rpm for 50 s to achieve semiconductor films of thickness 60 nm. All device fabrications and measurements were performed in air at room temperature.

**Fabrication of Conventional Photovoltaic Devices.** Bulk heterojunction (BHJ) OPV devices with ITO/PEDOT:PSS/polymer:$PC_{71}BM$/Ca/Al structures were fabricated. The ITO surface was cleaned by sonication and rinsing in distilled water, methanol, and acetone. A hole-transporting PEDOT:PSS layer (45 nm) was spin-coated onto each ITO anode from a solution purchased from Heraeus (CleviosTM P VP

AI4083), followed by spin-coating of a layer of polymer: $PC_{71}BM$; the polymer solution for spin-coating was prepared by dissolving the polymer (10 mg $mL^{-1}$) and $PC_{71}BM$ in a 97% chloroform/3% 1,8-diiodooctane (DIO), 97% chlorobenzene/3% DIO, or 97% *o*-dichlorobenzene (ODCB)/3% DIO mixture. Calcium and aluminum contacts were formed by vacuum deposition at pressures below $3 \times 10^{-6}$ Torr, providing an active area of 9 $mm^2$.

**Fabrication of Inverted Photovoltaic Devices.** Inverted BHJ OPV devices with ITO/PEIE (ethoxylated polyethylenimine)/polymer:$PC_{71}BM$/$MoO_3$/Ag structures were fabricated. The precleaned ITO substrates were treated with UV–ozone. The PEIE solution was spin-coated onto ITO substrates at a speed of 5000 rpm for 1 min, with an acceleration of 1000 rpm $s^{-1}$, and annealed at 120 °C for 10 min on a hot plate in ambient air. The PEIE thickness was estimated to be 10 nm. The substrates were then transferred into a nitrogen-filled glove box. The active layer of polymer:$PC_{71}BM$ (97% chlorobenzene/3% DIO mixture) was prepared by spin-coating at a speed of 1000 rpm for 30 s. The device was solvent-annealed for 1h at ambient temperature in the glove box. The device fabrication was completed by thermal evaporation of 10 nm $MoO_3$ and 100 nm Ag as the anode, under vacuum, at a base pressure of $3 \times 10^{-6}$ Torr. The effective area of the device was 9 $mm^2$.

**Measurement of Organic Photovoltaic Devices.** The thickness of the active layer was measured using a KLA Tencor Alpha-step IQ surface profilometer with an accuracy of ± 1 nm. The current-density–voltage (*J–V*) characteristics of the polymer photovoltaic cells were determined by illuminating the cells with simulated solar light (AM 1.5G) at an intensity of 100 mW $cm^{-2}$, using an Oriel 1000 W solar simulator. Electronic data were recorded using a Keithley 236 source-measure unit, and all characterizations were carried out under ambient conditions. The illumination intensity was calibrated using a standard silicon photodiode detector from PV Measurements Inc., which was calibrated at the National Renewable Energy Laboratory. The external quantum efficiency (EQE) was measured as a function of the wavelength in the range 360–800 nm, using a halogen lamp as the light source; calibration was performed using a silicon reference photodiode. The measurements were carried out after masking all but the active cell area of the fabricated device. All characterizations were performed under ambient conditions.

## Results and Discussion

**Polymer Synthesis and Characterization.** The synthetic route for the preparation of the polymer PTIPSBDT–DFDTBTz is shown in Scheme 1. PTIPSBDT–DFDTBTz was synthesized by the polycondensation of TIPSBDT and the corresponding dibrominated DFDTBTz via a palladium-catalyzed Stille reaction. The crude polymers were extracted with chloroform, collected by precipitation in methanol, and successively extracted with methanol and acetone, using a Soxhlet apparatus, to remove the byproducts. The number-average molecular-weight of the synthesized polymer was determined by GPC against polystyrene standards in a chloroform eluent, and was found to be 20 000 g $mol^{-1}$, with a polydispersity index of 2.5. The thermal stability of the polymer was investigated using TGA. This showed that the 5% weight-loss temperature of PTIPSBDT–DFDTBTz was 400 °C (Figure 1). This indicates that the thermal stability of PTIPSBDT–DFDTBTz is sufficient for use in optoelectronic devices. Differential scanning calorimetry showed no obvious exothermic and endothermic peaks in the temperature range from 25 to 250 °C, indicating that the film morphology should be stable over a wide temperature range (Figure 1: inset).

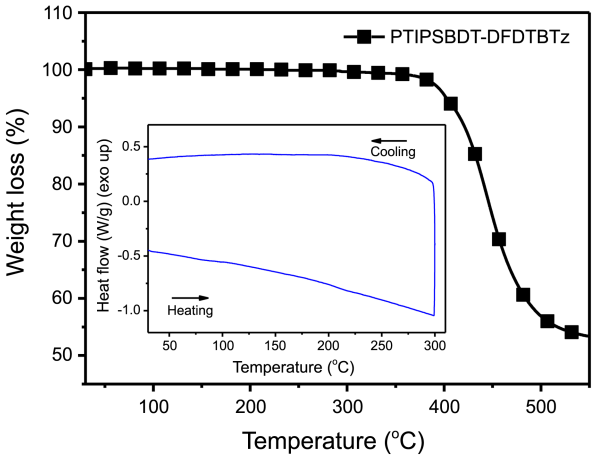


**Figure 1.** Thermogravimetric curves for PTIPSBDT–DFDTBTz at ramping rate of 10 °C $min^{-1}$; inset: DSC thermograms of PTIPSBDT-DFDTBTz under nitrogen.

**Optical and Electrochemical Properties.** Figure 2(a) shows the UV-visible absorption spectra of a dilute polymer solution in chloroform and a thin film spin-coated on a quartz substrate. The polymer solution and film display similar absorption bands with well-defined peaks and steep absorption edges. The absorption edge of the PTIPSBDT–DFDTBTz film is at 620 nm, corresponding to an optical band gap of 2.00 eV. Interestingly, the polymer film shows

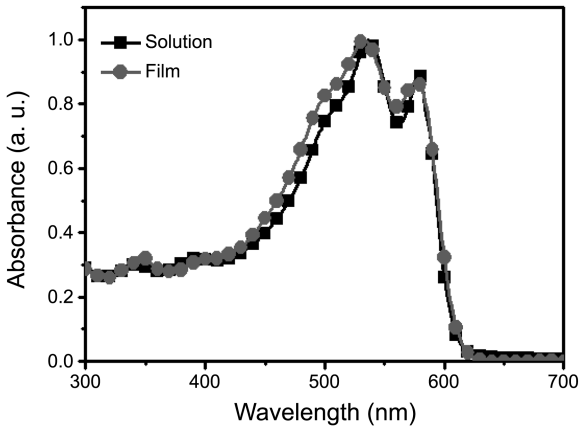


**Figure 2.** UV-visible absorption spectra of PTIPSBDT–DFDTBTz in chloroform solution and film state.

well-defined absorption spectra, indicating that the polymer has a somewhat ordered structure. The shape of the absorption band of the PTIPSBDT–DFDTBTz film is similar to that of a P3HT film ($E_g$ ~1.9 eV), but the absorption band of PTIPSBDT–DFDTBTz is slightly blue-shifted compared with that of P3HT. CV was used to determine the HOMO and lowest unoccupied molecular orbital (LUMO) energy levels of PTIPSBDT–DFDTBTz. CV was performed in an argon atmosphere in a solution of $TBABF_4$ (0.10 M) in acetonitrile at room temperature, using a scan rate of 50 mV $s^{-1}$. A platinum plate, platinum wire, and $Ag/Ag^+$ electrode were used as the working, counter, and reference electrodes, respectively. The HOMO energy level was determined by measuring the oxidation onsets ($E_{ox}$) of the polymer film.

To obtain the oxidation potential of the polymer film, the reference electrode was calibrated with ferrocene/ferrocenium, which has a redox potential with an absolute energy level of −4.80 eV in a vacuum; the potential of this external standard under the experimental conditions was 0.092 V *vs.* $Ag/Ag^+$. The HOMO energy values (EHOMO) were calculated using the following equation: $EHOMO = -e(E_{ox}^{onset} + 4.71)$ eV, where Eoxonset is the onset oxidation potential versus $Ag/Ag^+$. As shown in the CV curve of PTIPSBDT–DFDTBTz [Figure 3(a)], the onset oxidation potential is 0.88 V *vs.* $Ag/Ag^+$. The calculated HOMO energy level of PTIPSBDT–DFDTBTz is −5.59 eV. Fluorine is a strongly electron-withdrawing substituent, so its introduction into the conjugated backbone lowers both the HOMO and LUMO energy levels of conjugated polymers.[16] The LUMO energy level of the polymer was determined by combining the HOMO energy level data obtained from CV and the optical band gap energy data obtained from the absorption edge. Accordingly, the LUMO energy level of the polymer was estimated to be −3.59 eV. The polymer structure and corresponding energy levels are shown in Figure 3(b).

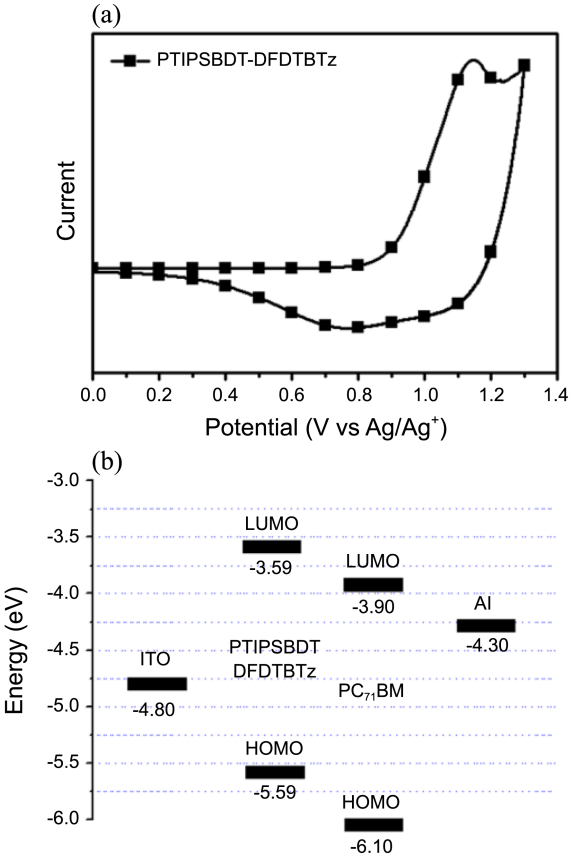


**Figure 3.** (a) Cyclic voltammograms of PTIPSBDT–DFDTBTz and (b) energy band diagrams of active materials and electrodes for photovoltaic devices.

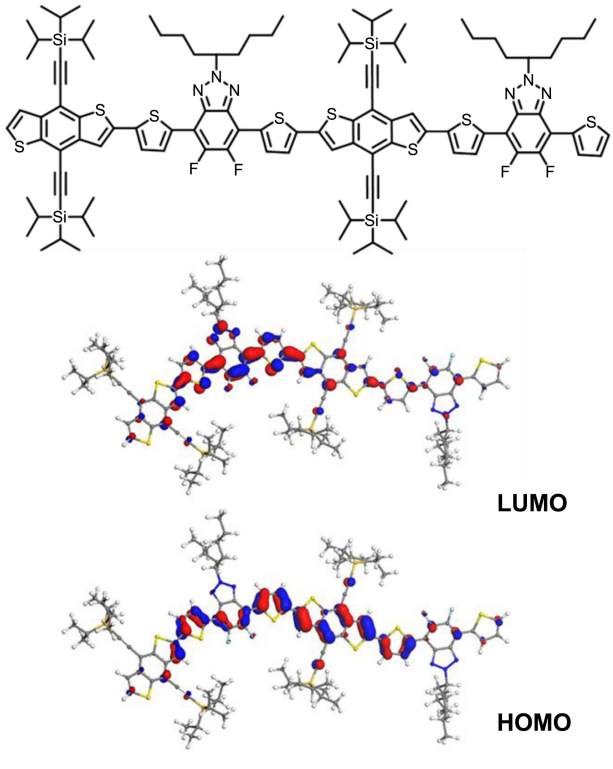


**Figure 4.** Chemical structures and electron distributions of frontier molecular orbitals of model compounds.

**Density Functional Theory Calculations.** The intramolecular charge transfer between the D–A–D–A charge transfer states, geometry, and electron state density were investigated using density functional theory calculations with DMol3 software.[17] In the DMol3 electronic structure calculation, the all-electron treatment and double numerical polarized basis sets were chosen. The density function was treated with the generalized gradient approximation, with the Perdew–Burke–Ernzerhof exchange correlation potential.[18] The results predicted that the HOMO was delocalized over the polymer backbone, whereas the LUMO was fairly well localized at the electron acceptor site. This configuration is generally observed for D–A-type polymers with push–pull units. The chemical structures of the model compounds and electron distribution of the frontier molecular orbitals are shown in Figure 4.

**Two-dimensional Grazing-incidence X-ray Scattering (2D-GIXS) and Structural Properties.** 2D-GIXS measurements were conducted to probe the crystallinity and crystal orientation of the polymer film. The samples were prepared

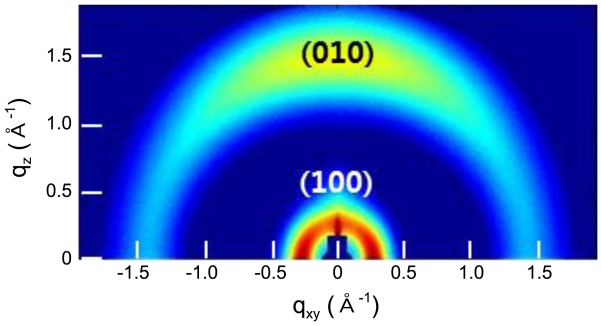


**Figure 5.** 2D-GIXS images of PTIPSBDT-DFDTBTz films.

by spin-coating polymer solutions onto PEDOT:PSS (40–50 nm)-coated Si wafers. Figure 5 shows the 2D-GIXS images of the PTIPSBDT-DFDTBTz film. The GIXS pattern of the PTIPSBDT-DFDTBTz film showed intense diffraction peaks at both $q_{xy}$ and $q_z$ ($q_z$ = 0.25 Å$^{-1}$), which correspond to the (100) reflection of the polymer crystal with a lamellar domain spacing ($d_1$) of 2.51 nm. The PTIPSBDT-DFDTBTz film also showed a strong (010) π–π stacking peak at around 1.72 Å$^{-1}$ which corresponds to a $d_{010}$ of 0.36 nm. This is a typical π–π stacking distance in donor-acceptor conjugated polymers with good photovoltaic performances.[19] It can be concluded that the PTIPSBDT-DFDTBTz chains in the film are predominantly arranged with a face-on orientation to the substrate.

**Thin-Film Transistor Characteristics of Polymer Thin Films.** The field-effect carrier mobility of the polymer was investigated by fabricating TFTs with a bottom-contact geometry, using an OTS-8-treated silicon dioxide dielectric and Au source–drain electrodes. The TFT mobilities were calculated in the saturation region, using the following equation:

$$I_{ds} = (WC_i/2L)\mu(V_G - V_T)^2$$

where $I_{ds}$ is the drain–source current in the saturated region, W and L are the channel width (120 μm) and length (12 μm), respectively, μ is the field-effect mobility, $C_i$ is the capacitance per unit area of the insulation layer (silicon dioxide, 300 nm), and $V_G$ and $V_T$ are the gate and threshold voltages, respectively.[20,21] Photocurrent loss in OPVs can be mitigated by increasing the charge carrier mobility, to achieve high-performance OPV devices. Figure 6 shows plots of Ids as a function of the source–drain voltage at different gate voltages from 0 to −60 V, and typical output and transfer curves for the polymer. The polymer TFTs exhibited typical p-channel TFT characteristics, with good drain–current modulation and well-defined linear and saturation regions. The OTFT fabricated using PTIPSBDT–DFDTBTz showed a hole mobility of 3.8 × 10$^{-3}$ cm$^2$V$^{-1}$s$^{-1}$.

**Photovoltaic Properties.** OPV cells were fabricated using PTIPSBDT–DFDTBTz as the electron donor and $PC_{71}BM$ as the electron acceptor, with the conventional device structure ITO/PEDOT:PSS/polymer:$PC_{71}BM$/Ca/Al, as shown in Figure 7(a). The performances of the prepared OPVs were strongly affected by the processing parameters, including the

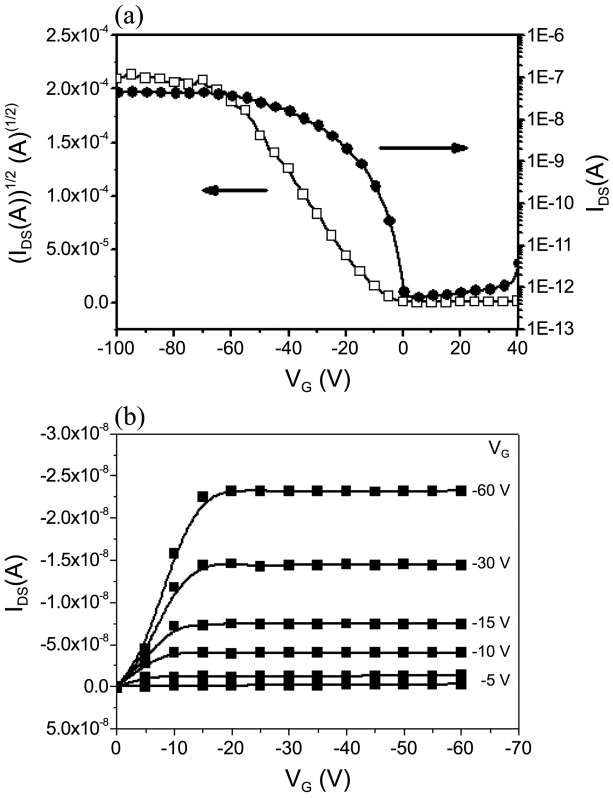


**Figure 6.** (a) Transfer characteristics of organic thin-film transistors fabricated using PTIPSBDT–DFDTBTz as active layer at a constant source–drain voltage of −80 V and (b) output curves of organic thin-film transistors.

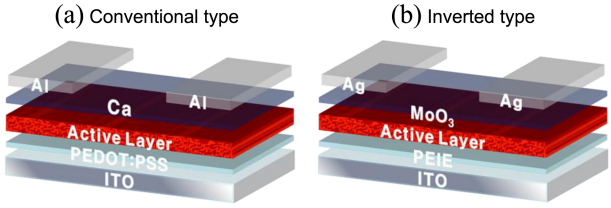


**Figure 7.** Device structures of fabricated (a) conventional and (b) inverted organic photovoltaic cells.

choice of solvent, blend ratio of the polymer and $PC_{71}BM$, and the processing additive. The photovoltaic performance of PTIPSBDT–DFDTBTz was investigated under various conditions. The active layers were spin-coated from a chlorobenzene solution of the donor polymer and acceptor, with 1,8-diiodooctane (DIO) as a processing additive to optimize the morphology of the active layer.

Figure 8(a), (b), and (c) shows the *J*−*V* characteristics of OPVs based on PTIPSBDT–DFDTBTz/$PC_{71}BM$ prepared with different composite ratios, solvents, and cell structures, under illumination of AM 1.5G, 100 mW cm$^{-2}$. To find the optimum polymer/acceptor ratio, the composite ratio was changed in the same processing solvent (chloroform/3 vol % DIO). The maximum PCE, 2.60%, was obtained with a 1:1 composite ratio. Three different processing solvents, namely chloroform (CF), chlorobenzene (CB), and *o*-dichlorobenzene (ODCB), were also tested to find a good processing

**Table 1.** Photovoltaic parameters of polymer measured under the illumination of simulated AM 1.5G conditions (100 mW/cm$^2$)

| Condition Solvent | Ratio | $V_{oc}$ [V][a] | $J_{sc}$ [mA/cm$^2$][a] | FF[a] | *PCE* [%][a] |
|---|---|---|---|---|---|
| CF+3 vol %DIO | 2:1 | 0.82 | 7.74 | 0.40 | 2.53 |
| | 1:1 | 0.85 | 8.09 | 0.38 | 2.60 |
| | 1:2 | 0.84 | 7.43 | 0.38 | 2.37 |
| Condition Polymer/$PC_{71}BM$ | Solvent With 3 vol % DIO | $V_{oc}$ [V][b] | $J_{sc}$ [mA/cm$^2$][b] | FF[b] | *PCE* [%][b] |
| 1:1 (w/w) | CF | 0.85 | 8.09 | 0.38 | 2.60 |
| | CB | 0.85 | 7.60 | 0.44 | 2.86 |
| | ODCB | 0.85 | 6.92 | 0.45 | 2.61 |
| Condition CB+3 vol %DIO | Cell Type | $V_{oc}$ [V] | $J_{sc}$ [mA/cm$^2$] | FF | *PCE* [%] |
| Polymer/$PC_{71}BM$ 1:1 (w/w) | Conventional | 0.85 | 7.60 | 0.44 | 2.86 |
| | Inverted[c] | 0.89 | 6.81 | 0.48 | 2.92 |

[a]Photovoltaic properties of copolymers/$PC_{71}BM$-based devices spin-coated from a chloroform (with 3 vol % DIO) solution for polymer. [b]Comparison of the photovoltaic properties of the OPVs based on polymer:$PC_{71}BM$ (1:1 with 3 vol % DIO) with different solvents. [c]ITO/PEIE/polymer:$PC_{71}BM$ (1:1 w/w)/$MoO_3$/Ag configuration.

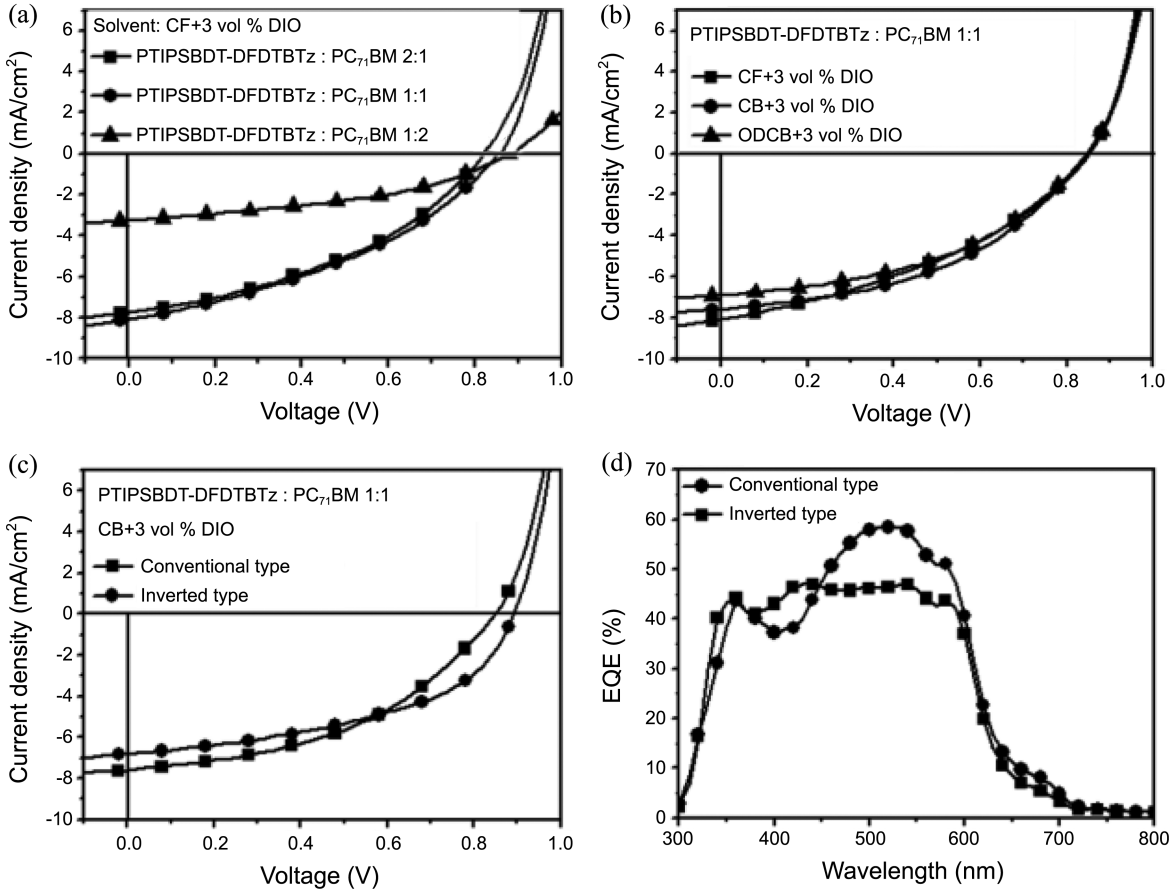


**Figure 8.** Current-density–voltage (*J–V*) curves of OPV devices fabricated using (a) PTIPSBDT–DFDTBTz:$PC_{71}BM$ (processed with 3 vol % DIO) in different weigh ratios and (b) PTIPSBDT–DFDTBTz:$PC_{71}BM$ (1:1, w/w, processed with 3 vol % DIO), using different processing solvents. (c) *J–V* curves of conventional and inverted OPV devices fabricated using PTIPSBDT–DFDTBTz:$PC_{71}BM$ (processed with chlorobenzene/3 vol % DIO). (d) EQE curves of conventional (circles) and inverted (squares) OPV devices.

solvent with the same active layer composition (1:1). The maximum PCE of 2.86% was obtained when chlorobenzene and a 1:1 composite ratio were used as the processing solvent and optimum composite ratio, respectively. The $V_{oc}$, $J_{sc}$, and fill factor (FF) of the fabricated conventional OPV were 0.85 V, 7.60 mA cm$^{-2}$, and 0.44, respectively. The relatively high $V_{oc}$ of the device agrees well with the measured low-lying HOMO energy level (−5.59 eV) of the PTIPSBDT −DFDTBTz donor. Inverted OPVs are known to have better long-term ambient stability than conventional OPVs, because

a stable high-work-function metal is used as the top electrode and the acidic PEDOT:PSS buffer layer on ITO is replaced by a stable cathode buffer layer.[22] In this study, we also fabricated an inverted OPV cell with the structure ITO/PEIE)/PTIPSBDT–DFDTBTz:$PC_{71}BM$ (1:1)/$MoO_3$/Ag, as shown in Figure 7(b). The fabricated inverted device exhibited a maximum PCE of 2.92%, with a $V_{oc}$ of 0.89 V, $J_{sc}$ of 6.81 mA $cm^{-2}$, and *FF* of 0.48. The $J_{sc}$ of the inverted device is slightly lower, but the $V_{oc}$ and *FF* are higher, than those of conventional devices. The performances of the fabricated conventional and inverted OPV cells are summarized in Table 1.

Figure 8(d) shows the EQE curves of conventional and inverted OPV devices fabricated under the same optimized conditions as those used for the *J–V* measurements. The $J_{sc}$ values were calculated by integrating the EQE data with the AM 1.5 G reference spectrum to evaluate the accuracy of the measurements. The $J_{sc}$ values obtained via integration of the EQE data and the *J*−*V* measurements are quite similar. In addition, the spectral responses of the OPV devices showed that photons within the range 350–700 nm contributed significantly to the EQE, with maximum EQEs of 55% (at 550 nm) and 50% (at 550 nm) for the conventional and inverted devices, respectively.

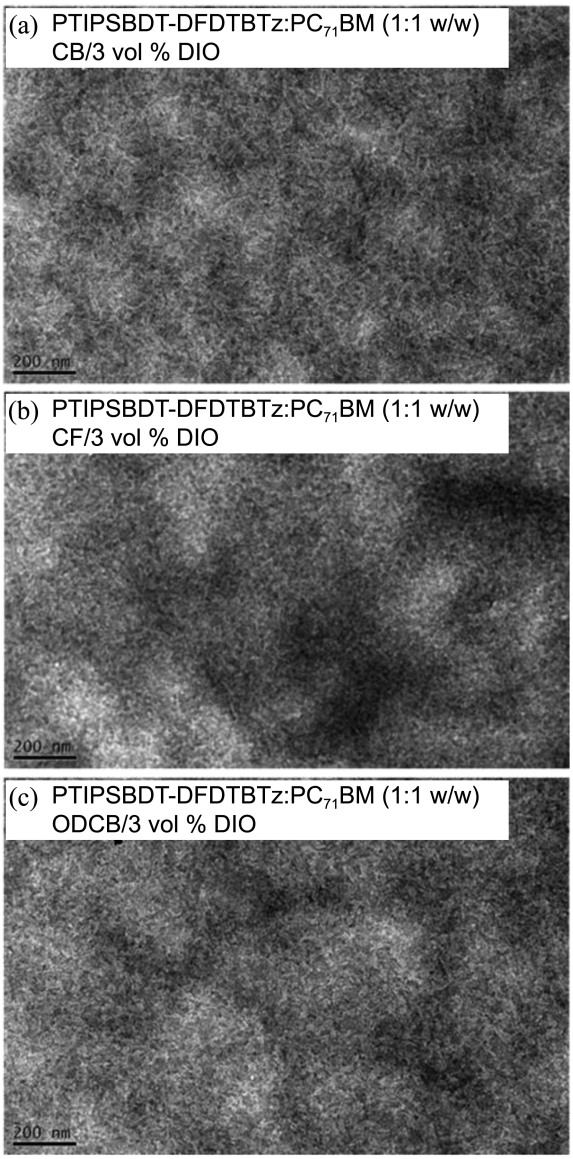


**Figure 9.** TEM images of polymer/$PC_{71}BM$ blends [1:1 w/w processed with 3 vol % DIO] cast from different solvents: (a) PTIPSBDT–DFDTBTz/$PC_{71}BM$ (1:1) CB/3 vol % DIO (200 nm scale); (b) PTIPSBDT–DFDTBTz/$PC_{71}BM$ (1:1) CF/3 vol % DIO (200 nm scale); and (c) PTIPSBDT–DFDTBTz/$PC_{71}BM$ (1:1) ODCB/3 vol % DIO (200 nm scale).

The morphologies of the active layers cast from different solvents were observed using transmission electron microscopy; the images are shown in Figure 9. The active layer cast from CB/DIO showed a very smooth surface, without distinct phase separation between the polymer and $PC_{71}BM$. In particular, a nanoscale interconnected network structure between the fibril-like polymer and $PC_{71}BM$ is well developed in the film cast from CB/DIO solvent, whereas the dark $PC_{71}BM$ phase becomes dominant and the density of the polymer fibrils becomes low in the films cast using other solvents (CF/DIO and ODCB/DIO).

## Conclusion

In summary, we successfully designed and synthesized a new D−A-type medium band gap copolymer, PTIPSBDT–DFDTBTz, through a Stille coupling reaction. Preliminary studies of the copolymer showed a hole mobility as high as $3.8 \times 10^{-3}$ $cm^2$ $V^{-1}$ $s^{-1}$ in an OTFT, and a HOMO energy level at −5.59 eV. The OPV device with a conventional device structure fabricated using PTIPSBDT–DFDTBTz:$PC_{71}BM$ exhibited a PCE of 2.86%, and inverted OPVs with the same active layer exhibited a maximum PCE of 2.92%.

**Acknowledgments.** This work was supported by the New and Renewable Energy Program of the Korea Institute of Energy Technology Evaluation and Planning (KETEP), funded by the Ministry of Knowledge Economy (MKE) (20113010010030), a NRF grant funded by the Korean Government (NRF-2013-Global Ph.D. Fellowship Program), and an NRF grant funded by the Korea government (MSIP) through GCRC-SOP (No. 2011-0030013).

## References

1. (a) Chen, H.-Y.; Hou, J. H.; Zhang, S. Q.; Liang, Y.; Yang, G. W.; Yang, Y.; Yu, L. P.; Wu, Y.; Li, G. *Nat. Photonics* **2009**, *3*, 649. (b) Yu, G.; Gao, J.; Hummelen, J. C.; Wudl, F.; Heeger, A. J. *Science* **1995**, *270*, 1789.
2. (a) Wienk, M. M.; Koon, J. M.; Verhees, W. J. H.; Knol, J.; Hummelen, J. C.; Van Hal, P. A.; Janssen, R. A. J. *Angew. Chem., Int. Ed.* **2003**, *42*, 3371. (b) Dennler, G.; Scharber, M. C.; Brabec, C. J. *Adv. Mater.* **2009**, *21*, 1323.
3. (a) Ning, W.; Chen, Z.; Wei, W.; Jiang, Z. *J. Am. Chem. Soc.* **2013**, *135*, 17060. (b) Zhang, M.; Guo, X.; Zhang, S.; Hou, J. *Adv. Mater.* DOI: 10.1002/adma.201304427.
4. Thompson, B. C.; Fréchet, J. M. J. *Angew. Chem., Int. Ed.* **2008**, *47*, 58.
5. Cheng, Y. J.; Yang, S. H.; Hsu, C. S. *Chem. Rev.* **2009**, *109*, 5868.
6. (a) Dou, L.; You, J.; Yang, J.; Chen, C. C.; He, Y.; Murase, S.;

Moriarty, T.; Emery, K.; Li, G.; Yang, Y. *Nat. Photonics* **2012**, *6*, 180. (b) Kim, J.-H.; Song, C. E.; Kang, I.-N.; Shin, W. S.; Hwang, D.-H. *Chem. Commun.* **2013**, 3248. (c) Kim, J.-H.; Kim, H. U.; Kang, I.-N.; Lee, S. K.; Moon, S.-J.; Shin, W. S.; Hwang, D.-H. *Macromolecules* **2012**, *45*, 8628.
7. Zhou, H.; Yang, L.; Stuart, A. C.; Price, S. C.; Liu, S.; You, W. *Angew. Chem., Int. Ed.* **2011**, *50*, 2995.
8. You, J. B.; Dou, L. T.; Yoshimura, K.; Kato, T.; Ohya, K.; Moriarty, T.; Emery, K.; Chen, C. C.; Gao, J.; Li, G.; Yang, Y. *Nat. Commun.* **2013**, *4*, 1446.
9. Li, Y. *Acc. Chem. Res.* **2012**, *45*, 723.
10. Zhou, H.; Yang, L.; You, W. *Macromolecules* **2012**, *45*, 607.
11. (a) Kim, J.-H.; Song, C. E.; Kim, H. U.; Grimsdale, A. C.; Moon, S.-J.; Shin, W. S.; Choi, S. K.; Hwang, D.-H. *Chem. Mater.* **2013**, *25*, 2722. (b) Dou, L.; Chang, W.-H.; Gao, J.; Chen, C.-C.; You, J.; Yang, Y. *Adv. Mater.* **2013**, *25*, 825.
12. (a) Dang, M. T.; Hirsch, L.; Wantz, G. *Adv. Mater.* **2011**, *23*, 3597. (b) Chang, C.-Y.; Wu, C.-E.; Chen, S.-Y.; Cui, C.; Cheng, Y.-J.; Hsu, C. S.; Wang, Y.-L.; Li, Y. *Angew. Chem., Int. Ed.* **2011**, *50*, 9386. (c) Zhong, H.; Li, Z.; Deledalle, F.; Fregoso, E. C.; Shahid, M.; Fei, Z.; Nielsen, C. B.; Yaacobi-Gross, N.; Rossbauer, S.; Anthopoulos, T. D.; Currant, J. R.; Heeney, M. *J. Am. Chem. Soc.* **2013**, *135*, 2040. (d) Dou, L.; Chang, W.-H.; Gao, J.; Chen, C.-C.; You, J.; Yang, Y. *Adv. Mater.* **2013**, *25*, 825.
13. Kim, J.-H.; Song, C. E.; Shin, N.; Kang, H.; Wood, S.; Kang, I.-N.; Kim, B. J.; Kim, B. S.; Kim, J.-S.; Shin, W. S.; Hwang, D.-H. *ACS Appl. Mater. Interfaces* **2013**, *24*, 12820.
14. Kim, J.-H.; Kim, H. U.; Song, C. E.; Kang, I.-N.; Lee, J.-K.; Shin, W. S.; Hwang, D.-H. *Solar Energy Materials & Solar Cells* **2013**, *108*, 113.
15. Shin, S. A.; Kim, J.-H.; Park, J. B.; Kang, I.-N.; Park, M.-J.; Hwang, D.-H. *Macromol. Chem. Phys.* **2013**, *214*, 1780.
16. Price, S. C.; Stuart, A. C.; Yang, L.; Zhou, H.; You, W. *J. Am. Chem. Soc.* **2011**, *133*, 4625.
17. Perdew, J. P.; Wang, Y. *Phys. Rev. B* **1992**, *45*, 13244.
18. Perdew, J. P.; Burke, K.; Ernzerhof, M. *Phys. Rev. Lett.* **1996**, *77*, 3865.
19. Cho, H.-H.; Kang, T. E.; Kim, K.-H.; Kang, H.; Kim, H. J.; Kim, B. *Macromolecules* **2012**, *45*, 6415.
20. Shaw, J. M.; Seidler, P. F. *IBM J. Res. Dev.* **2001**, *45*, 3.
21. Dimitrakopoulos, C. D.; Mascaro, D. J. *IBM J. Res. Dev.* **2001**, *45*, 11.
22. Kim, K.-H.; Kang, H.; Kim, H. J.; Kim, P. S.; Yoon, S. C.; Kim, B. J. *Chem. Mater.* **2012**, *24*, 2373.